Article

Evaluation of Compounds from *Balanites aegyptiaca* against Squalene Epoxidase of *Micropsorum gypseum*—In Vitro and In Silico Studies

Mohamed Husain Syed Abuthakir [1,2], V. Hemamalini [1], Reham M. Alahmadi [3], Anis Ahamed [3], Ashraf Atef Hatamleh [3], Razack Abdullah [4] and Jeyam Muthusamy [1,*]

[1] Department of Bioinformatics, Bharathiar University, Coimbatore 641046, Tamil Nadu, India; biothakir@gmail.com (M.H.S.A.); hemamalini@buc.edu.in (V.H.)
[2] Institute of Systems Biology, Universiti Kebangsaan Malaysia, Bangi 43600, Selangor, Malaysia
[3] Department of Botany and Microbiology, College of Science, King Saud University, P.O. Box 2455, Riyadh 11451, Saudi Arabia; realahmadi@ksu.edu.sa (R.M.A.); anazeer@ksu.edu.sa (A.A.); ahatamleh@ksu.edu.sa (A.A.H.)
[4] Law Sau Fai Institute for Advancing Translational Medicine in Bone and Joint Diseases, School of Chinese Medicine, Hong Kong Baptist University, Kowloon, Hong Kong, China; sheikmod@gmail.com
[*] Correspondence: jeyam@buc.edu.in

Abstract: *Microsporum gypseum* is a dermatophyte with a geophilic nature that is found all over the globe. It mainly causes tinea in the scalp, arms, and legs in humans. Squalene epoxidase (SE) is a crucial enzyme in *M. gypseum* for the biosynthesis of ergosterol. The medicinal plant *Balanites aegyptiaca* is an abundant supply of secondary constituents with great therapeutic values. In this research, the fruit epicarp portion was used to inhibit *M. gypseum* using experimental and computational techniques. The anti-dermatophytic activity of epicarp extracts on *M. gypseum* was evaluated using the poison plate method at five different concentrations. At 3 mg/mL, the *M. gypseum* was completely controlled by the fractioned chloroform extract of epicarp. The compounds from previous research were utilized for docking studies (Abuthakir et al., 2022). The ideal compounds and the drug terbinafine were then docked using Schrödinger's Glide module. It demonstrates that (3E)-7-Hydroxy-3,7-dimethyl-3-octen-1-yl-6-O-(6-deoxy-alpha-L-mannopyranosyl)-beta-D-glucopyranoside outperforms other substances and the drug terbinafine in docking analysis. Desmond, Schrödinger Molecular Dynamics simulations were also performed for (3E)-7-Hydroxy-3,7-dimethyl-3-octen-1-yl-6-O-(6-deoxy-alpha-L-mannopyranosyl)-beta-D-glucopyranoside-squalene epoxidase complexes. The complex appears to be more stable, according to the MD simulation research. This study indicates that (3E)-7-Hydroxy-3,7-dimethyl-3-octen-1-yl-6-O-(6-deoxy-alpha-L-mannopyranosyl)-beta-D-glucopyranoside could be used as a potential inhibitor of *M. gypseum* growth, and it could be studied further.

Keywords: dermatophytes; *Microsporum gypseum*; squalene epoxidase; docking; MD simulation

1. Introduction

Tinea, or dermatophytosis, is a superficial skin illness affected by dermatophytes, a cluster of filamentous fungus species [1]. These are everywhere worldwide, but they are more prevalent in warm, humid tropical and subtropical climate zones [2].

The colonies of the geophilic dermatophyte *Microsporum gypseum* develop in soil on keratinous substrates. This is an extremely important dermatophyte because it is involved in the degradation of keratin in the soil [3]. It is saprophytic and obtains enrichments from keratinized tissue substrates [4]. Dermatophytosis caused by *M. gypseum* primarily affects people who have direct contact with soil, such as farmers and gardeners, and it primarily causes tinea capitis, tinea corpus [5], and tinea corporis in humans [6]. Squalene epoxidase (SE) is a key enzyme for ergosterol biosynthesis in dermatophytes. Squalene

is transformed to 2,3-oxidosqualene by this monooxygenase, and fungal growth can be inhibited by blocking this enzyme [7].

Terbinafine and naftifine, both members of the Allylamine group, are efficient drug substances for inhibiting the activity of squalene epoxidase. Squalene accumulation increased in cell membranes due to squalene epoxidase inhibition, resulting in increased membrane permeability, disruption of cellular substances, and, finally, fungal death [8]. In indigenous medical systems all across the world, medicinal plants are crucial. Ethnobotany insight is a valuable resource for the development and research of medicines [9]. *B. aegyptiaca* has rich remedial properties and works as an herbaceous medication. Various components of *Balanites aegyptiaca* have powerful medicinal properties, including antihelmintic, anticancer, antimicrobial, antidiabetic, antiviral, and antioxidant agents. It is also used as a purgative and emetic, and it cures malaria, syphilis, skin boils, liver disorder, and leukoderma and revives wounds and pains [10]. This research concentrates on the antidermatophytic behavior of the medicinal plant *B. aegyptiaca* epicarp by blocking the evolvement of *Microsporum gypseum* using research investigation of distinctive compounds from the extract with energetic action using liquid chromatography–mass spectrometry, protein–ligand docking, and molecular dynamics simulation analysis.

2. Materials and Methods

2.1. Plant Species Collection and Identification

Balanites aegyptiaca was collected from the Nilambur region of Coimbatore district, Tamil Nadu, Southern India, and it is submitted to the Botanical Survey of Coimbatore in Tamil Nadu for plant authentication. The epicarp region was completely detached from the fruit, then shade-dried, ground, and orderly extracted with diverse chemical solvents comprising petroleum ether, hexane, chloroform, ethyl acetate, methanol, and water, in addition to direct methanol and water using the Soxhlet extraction method.

2.2. Purchasing Pathogen

Microsporum gypseum fungus culture MTCC.6041 was obtained from the MTCC (Microbial Type Culture Collection and Gene Bank) in Chandigarh for this study.

2.3. Anti-Dermatophytic Assay

The antidermatophytic exploit of different epicarp extracts on *M. gypseum* was evaluated using a poison plate assay [11]. Epicarp extracts were organized and put in SDA medium in a range of concentrations (1 mg/mL to 5 mg/mL), while a control plate was made without extract, and a positive control was made using the medication ketoconazole. Every day, the growth of mycelia of *M. gypseum* was monitored, and the inhibitory percentage (I) was calculated after 11 days of incubation using the method below.

$$I = \{(Dcontrol - Dtreated)/Dcontrol\} \times 100$$

The results of the experiments, which were run three times, were presented as the mean standard error (SE). The data were statistically analyzed using SPSS software version 20.

2.4. Minimum Inhibitory Concentration (MIC)

According to NCCLS (National Committee for Clinical Laboratory Standards) recommendations for filamentous fungi (M38-A2), two-fold broth dilution techniques were employed to determine the Minimum Inhibitory Concentration. *M. gypseum* culture, which was 21 days old, was used to prepare the inoculum, and spore suspension with 0.1 to 1.8×10^5 CFU/mL was developed for MIC [12].

The 90% inhibition was observed as MIC90; it was observed after 7 days of incubation at 30 °C at different concentrations from 50 mg/mL to 0.1 mg/mL.

2.5. Phytochemical Screening

The CHL extract of epicarp was further analyzed for screening phytochemicals using various investigations such as Benedict's test, Biuret test, frothing test, ferric chloride test, Mayer's test, KOH test, etc., to determine the presence of various phytochemicals [13].

2.6. Compound Elucidation

Liquid chromatography–mass spectrometry (LC–MS) detected the macromolecules and secondary compounds from the extract of epicarp. This study was executed using the UPLC-QToF-MS instrument [14]. The mass values of LC–MS-elucidated composites were matched with the GNPS (Global Natural Products Social Molecular Networking) library to find the exact compound [15].

2.7. Modeling and Validation of Protein

Atomic structure of squalene monooxygenase of *M. gypseum* was not found in PDB. Hence, the modeled protein was downloaded from the AlphaFold database. Then, the PROCHECK server, using the Ramachandran plot study, verified the modeled protein quality [16].

2.8. Binding Site Prediction

Binding site of the protein squalene monooxygenase of *M. gypseum* was predicted using the SiteMap module of Schrödinger [17]. In addition to that, the conserved residues were predicted using the Consurf server [18].

2.9. Ligand Preparation

In PubChem, the crystal structure of the drug naftifine and compounds of epicarp were obtained. Furthermore, these substances were assigned for ADME-Tox testing using the QikProp module [19]. Each compound's absorption, diffusion, metabolism, excretion, and toxicity were investigated [20].

2.10. Protein–Ligand Docking

The GLIDE module of Schrödinger was used to conduct docking studies for proteins and ligands [21]. This process included protein preparation, grid creation, ligand preparation, and docking ligand with protein. The first step began with protein preprocessing, which involved increasing hydrogen atoms, improving the amino acid orientation of hydroxyl groups and amide groups, and forming disulfide bonds. The OPLS3e force field was used to minimize energy, with non-hydrogen atoms being lowered until the common root-mean-square deviation (RMSD) achieved the standard value of 0.3.

A grid surrounded the important residues of squalene monooxygenase. The drug terbinafine and compounds from epicarp were created through an optimization procedure that employed the OPLS3e force field. Lastly, the molecular docking was carried out using the XP (extra precision) method [22,23] by incorporating the ligand preparation and grid generation output files.

2.11. MM-GBSA Analysis

Molecular mechanics with generalized Born surface area (MM-GBSA) analysis was carried out using the Prime module of Schrödinger for relative binding free energy calculation of protein–ligand complex. The selected docked complex structures were carried out for binding free energy calculation. The relative binding free energy ΔG_{bind} was calculated by the following equation [24],

$$\Delta G_{bind} = E_{complex} \text{ (minimized)} - [E_{ligand} \text{ (unbound, minimized)} + E_{receptor} \text{ (unbound, minimized)}]$$

2.12. Molecular Dynamics Simulation

Complex structure of squalene monooxygenase and ligand was tested for stability by Molecular Dynamics (MD) simulation method for 10 ns using Desmond component, Schrödinger [25].

The simulation procedure began with the Protein Preparation Wizard, which was used to optimize and minimize the docked structure using the OPLS3e force field. Furthermore, system builder was made with the use of the TIP3P solvent model, a cubic box shape with a reduced volume, and a 10 Å buffer area. The requisite positive (Na^+) and negative (Cl^-) ions were then added to the system, along with 0.15 M salt, to neutralize it. Using the system's built-in relaxation process, the system was minimized for 2000 iterations with a convergence threshold of 1 kcal/mol and pre-equilibrated [26].

Further, the results were evaluated using parameters such as protein–ligand RMSD, RMSF of protein and ligand, protein–ligand contacts, encompassing numerous kinds of interactions such as hydrogen bond interactions, which were crucial in determining the complex's stability.

3. Results

3.1. Plant Verification

The submitted plant (BSI/SRC/5/23/2018/Tech.1582) was authenticated by Dr. C. Murugan, Scientist 'D' Botanical Survey of India, Southern Regional Centre Coimbatore. The plant was identified as *Balanites aegyptiaca* (L.) Delile.

3.2. Anti-Dermatophytic Assay

The anti-dermatophytic activity (Figure 1) of different extracts of *Balanites aegyptiaca* on *Microsporum gypseum* was evaluated (Table 1).
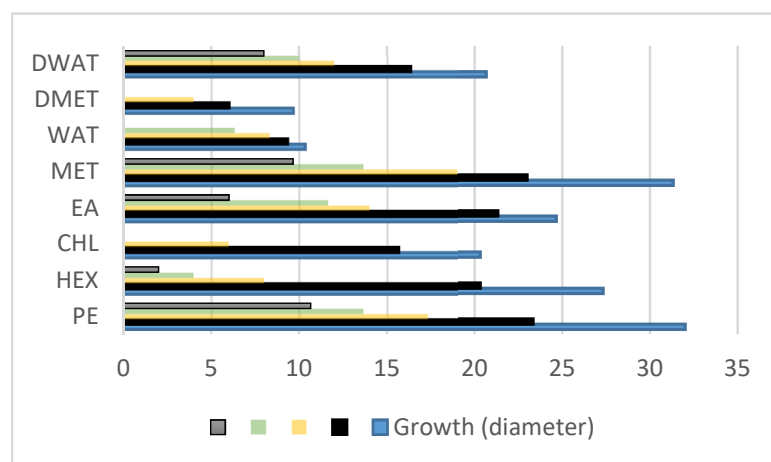

Figure 1. Mycelial growth of *Microsporum gypseum* inhibited by various extracts of epicarp of *Balanites aegyptiaca* (blue: 1 mg/mL, black: 2 mg/mL, yellow: 3 mg/mL, green: 4 mg/mL, and grey: 5 mg/mL).

Table 1. Efficacy of different extracts of fruit epicarp portion of *B. aegyptiaca* on *M. gypseum*.

Extracts		PE	HEX	CHL	EA	MET	WAT	DMET	DWAT
	1 mg/mL	32	27.33	20.33	24.66	31.33	10.33	9.66	20.66
	2 mg/mL	23.33	20.33	15.66	21.33	23	9.33	6	16.33
Growth (diameter)	3 mg/mL	17.33	8	6	14	19	8.33	4	12
	4 mg/mL	13.66	4	-	11.66	13.66	6.33	-	10
	5 mg/mL	10.66	2	-	6	9.66	-	-	8

After reviewing the top findings, it was discovered that fractionated CHL extract at 4 mg/mL completely inhibited mycelial growth of *M. gypseum* (Figure 2), fractioned water extract at 5 mg/mL and methanol (DMET) extract at 4 mg/mL completely inhibited mycelial growth of *M. gypseum*. Further study going on the fractioned CHL of fruit's epicarp section was concentrated on it because it was discovered to have stronger activity.
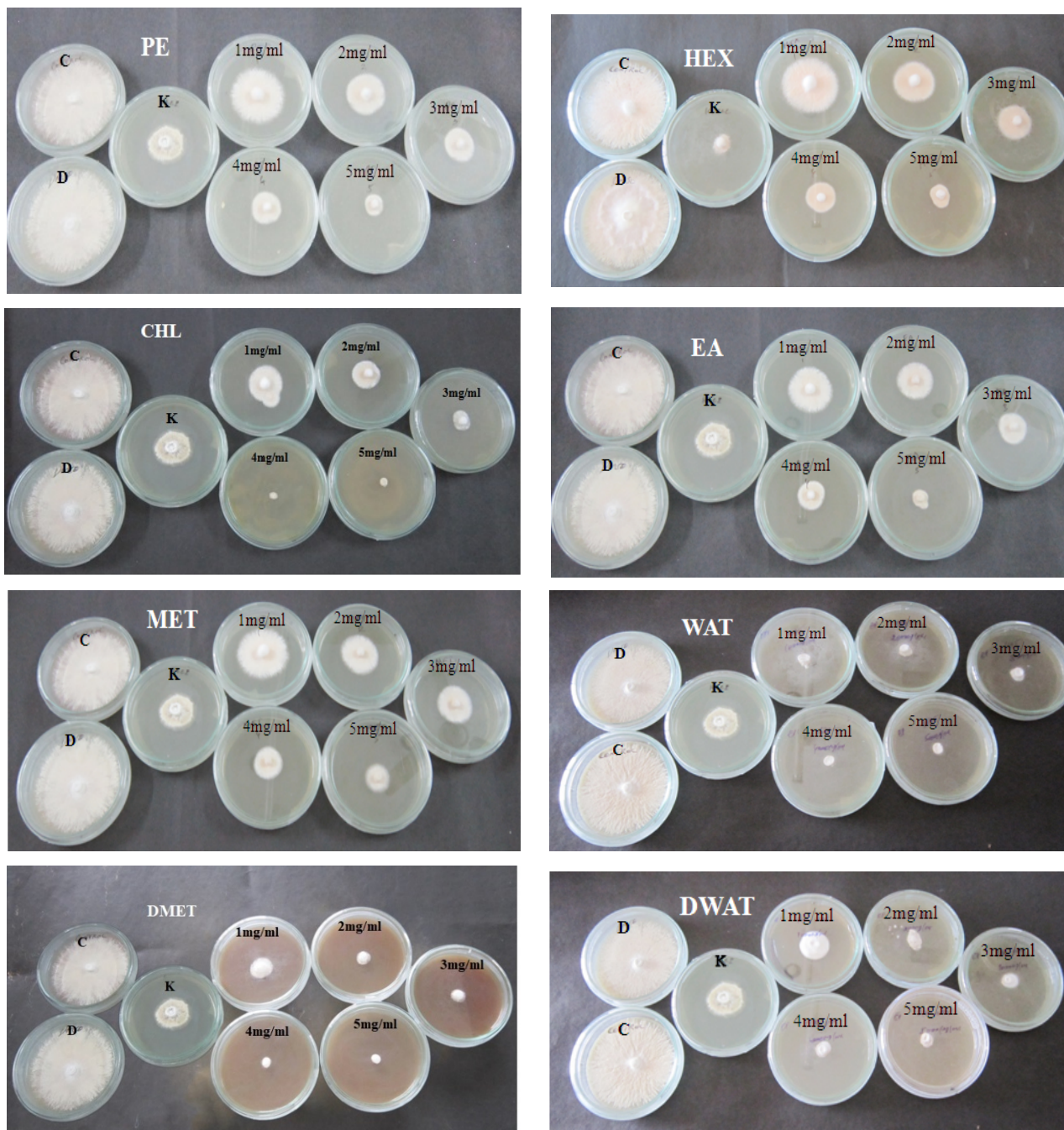

Figure 2. Anti-dermatophytic activity of various extracts of *B. aegyptiaca* epicarp on *M. gypseum*. C—control, D—DMSO, K—ketoconazole.

After an incubation period, the MIC_{90} was observed and was determined to have 90% inhibition since there was no observable development. The MIC_{90} for fractioned CHL extract of epicarp on *M. gypseum* was 3.12 mg/mL (Figure 3).
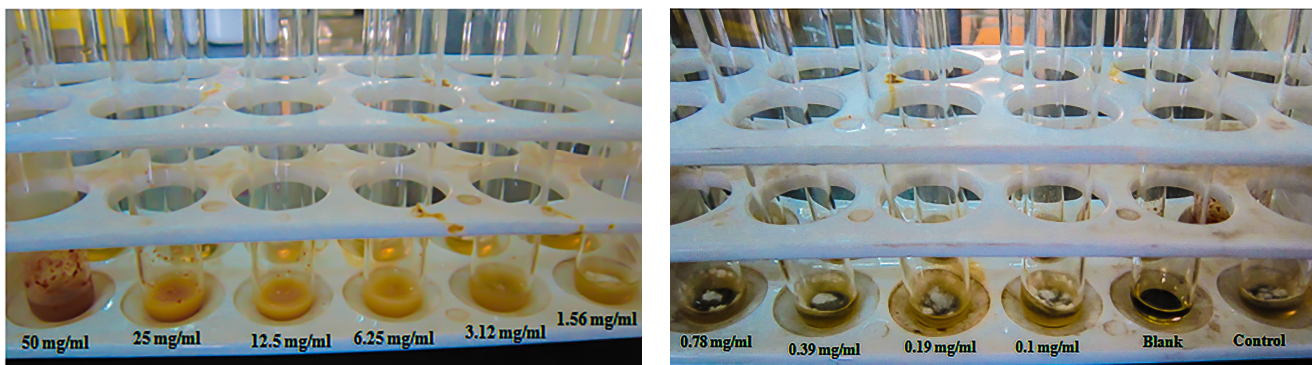
Figure 3. MIC result of *B. aegyptiaca* epicarp part fractionated chloroform extract on *M. gypseum*.

3.3. Phytochemical, LC–MS, and ADMETox Analysis

Phytochemical analysis (Supplementary Table S1) and LC–MS analysis of fractioned chloroform extract of fruit epicarp (Supplementary Figure S1), then those mass values were compared with GNPS database and compounds (Supplementary Table S2) were retrieved further ADMETox results (Supplementary Table S3) were reported in my previous article [27].

3.4. Modeling and Confirmation

The 3D structure of squalene monooxygenase of *M. gypseum* was downloaded using the AlphaFold database. The predicted protein structure (Figure 4a) of squalene monooxygenase was verified further, and the results showed that 92.8% of the residues were located in the area that was most preferred (Figure 4b).
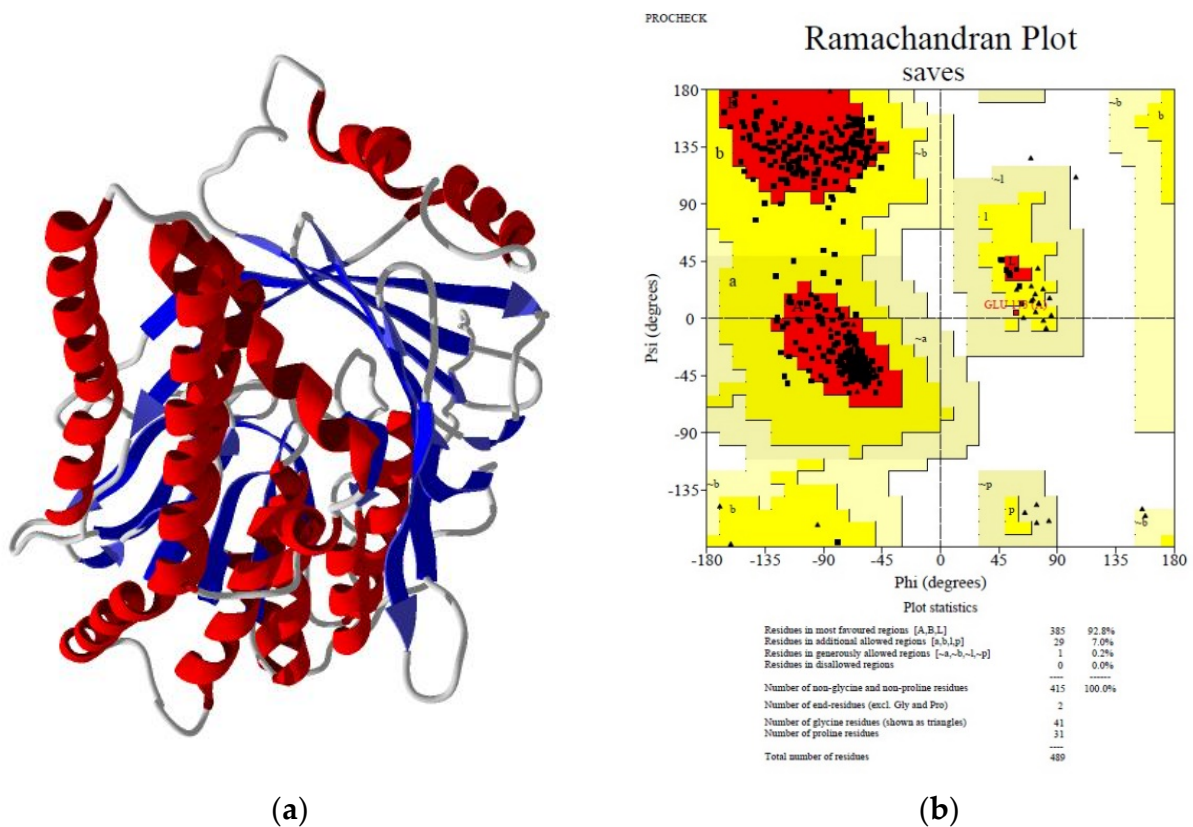

(**a**)

(**b**)

Figure 4. (**a**) Predicted 3D structure and (**b**) Ramachandran plot result of squalene monooxygenase of *M. gypseum*.

3.5. Binding Site Prediction

The binding site of squalene monooxygenase of *M. gypseum* was predicted, and the following residues were involved in the binding pocket (Figure 5a) with the values of site score 1.084 and druggable score 1.007. The Consurf server was used to forecast conserved residues, which are displayed in Figure 5b.
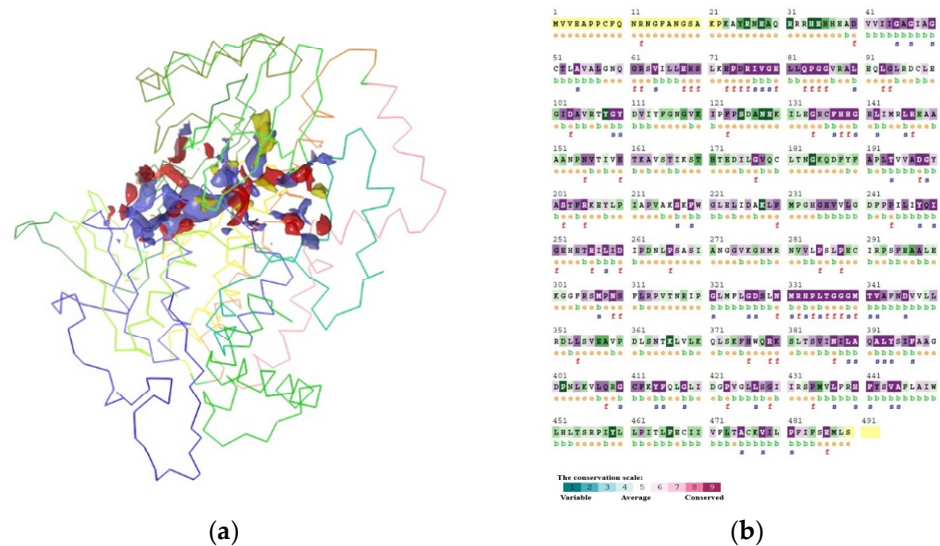

| (a) | (b) |

Figure 5. (**a**) Predicted binding site and (**b**) conserved residues of squalene monooxygenase of *M. gypseum* using sitemap and Consurf (s-structurally conserved, f-functionally conserved residues).

The predicted binding site residues of squalene monooxygenase of *M. gypseum* are I44, G45, A46, G47, I48, A49, G50, E68, R69, S70, P74, R76, I77, V78, G79, E80, L81, Q83, V105, T107, Y108, G109, Y110, D111, V112, I113, I121, C136, F137, H138, H139, G140, L142, I143, A197, D198, G199, Y200, E223, G235, H236, V237, P244, I245, L246, Y248, R256, L258, I259, D260, R305, M307, P308, N309, S310, L325, G326, D327, S328, L329, N330, M331, R332, H333, P334, L335, T336, G337, G339, M340, V342, A343, D346, T383, I386, F397.

3.6. Molecular Docking

Using XP (extra precision) docking, the 40 LC–MS-derived composites and naftifine drug were docked with the squalene epoxidase of *M. gypseum*. The molecules were discovered through docked complex structure analysis. (3E)-7-Hydroxy-3,7-dimethyl-3-octen-1-yl-6-O-(6-deoxy-alpha-L-mannopyranosyl)-beta-D-glucopyranoside (CID: 56776227), 2-phenyl-2-[(2S,3R,4S,5S,6R)-3,4,5-trihydroxy-6-[[(2R,3R,4S,5S,6R)-3,4,5-trihydroxy-6-(hydroxymethyl)oxan-2-yl]oxymethyl]oxan-2-yl]oxyacetamide (CID: 11248520), as well as platyphylloside (CID: 9826264) had the highest number of composites with interactions to important residues, and more than 12 compounds had a good result than the medication naftifine (Table 2).

Naftifine drug had a −7.1 kcal/mol docking score and contacts with the binding site residues Pro 334 and Phe 397. Epicarp's plant composite 56776227 had a docking score of −10.1 kcal/mol and bonded with structurally conserved residues Val 78, Gly 109, Tyr 110, functionally conserved residue Glu 80, and binding site residues Asp 111 and Val 112 (Figure 6). The plant composite 11248520 interacted with structurally conserved residues Val 78 and functionally conserved residues Glu 80 and Pro 334 with a docking score of −9.8 kcal/mol. The compound 9826264 had a −9.2 kcal/mol docking score and contacts with binding site residue Pro 224, structurally conserved residue Phe 397, and functionally conserved residues Glu 80, Thr 336, and Met 340. The compounds obtained from the epicarp of fruit *B. aegyptiaca* demonstrated more effective anti-dermatophytic activity as opposed to the squalene epoxidase.

Table 2. Docking results of squalene monooxygenase of *M. gypseum* with compounds derived from fractioned CHL extract of *B. aegyptiaca*'s fruit epicarp.

| Compound No.	Compound Name	Docking Score (kcal/mol)	Interacting Residues	Bond Length (Å)
1.	(3E)-7-Hydroxy-3,7-dimethyl-3-octen-1-yl 6-O-(6-deoxy-alpha-L-mannopyranosyl)-beta-D-glucopyranoside	−10.1	Val 78, Glu 80, Gly 109, Tyr 110, Asp 111, Val 112	1.81, 2.29, 2.08, 3.12, 2.14, 1.86
2.	2-phenyl-2-[(2S,3R,4S,5S,6R)-3,4,5-trihydroxy-6-[[(2R,3R,4S,5S,6R)-3,4,5-trihydroxy-6-(hydroxymethyl)oxan-2-yl]oxymethyl]oxan-2-yl]oxyacetamide	−9.8	Val 78, Glu 80(3), Pro 334	1.72, 1.65, 2.07, 2.45, 1.67
3.	Platyphylloside	−9.2	Glu 80, Pro 224, Thr 336, Met 340, Phe 397	2.09, 2.56, 2.61, 2.05, 4.98
5.	Forchlorfenuron	−8.8	Glu 80, Arg 256, Pro 340(2), Phe 397	2.57, 5.35, 1.89, 2.12, 5.01
6.	1,3,6-trihydroxy-5-methoxy-2-[(2S,3R,4R,5S,6R)-3,4,5-trihydroxy-6-(hydroxymethyl)oxan-2-yl]xanthen-9-one	−8.5	Val 78, Glu 80, Leu 81, Thr 336	2.04, 2.07, 2.53, 2.17
7.	Thelephoric acid	−7.9	Val 78(2), Arg 256	1.83, 2.23, 1.92
8.	4-[(2-{[(2-Ethyl-2,3-dihydroxybutanoyl)oxy]methyl}phenyl)amino]-4-oxobutanoic acid	−7.7	Val 78, Val 112, Gly 235, Pro 334, Thr 336	1.85, 1.91, 1.95, 1.82, 2.71
9.	N-Acetyl-D-Galactosamine	−7.6	Glu 80, Pro 334, Thr 336, Gly 337	2.60, 2.08, 2.18, 2.57
10.	N~5~-Carbamoyl-N~2~-(phenylacetyl)ornithine	−7.4	Gly 109, Gly 235, Pro 334, Gly 337, Phe 397	2.04, 2.35, 2.11, 1.97, 4.90
11.	N-[2-(4-sec-Butyl-phenoxy)-4,5-dihydroxy-6-hydroxymethyl-tetrahydro-pyran-3-yl]-acetamide	−7.3	Glu 80(2), Arg 256	2.15, 2.24, 2.12
12.	2-[5-[2-[2-[5-(2-oxopropyl)oxolan-2-yl]propanoyloxy]butyl]oxolan-2-yl]propanoic acid	−7.2	Thr 336, Gly 337, Gly 339, Met 340	2.04, 2.76, 1.70, 2.11
13.	Naftifine	−7.1	Pro 334, Phe 397	2.06, 4.88
14.	3-[(E)-2-(3-Hydroxyphenyl)ethenyl]-5-methoxyphenol	−7.1	Leu 258, Phe 397	1.64, 5.03
15.	N-Acetylneuraminate	−6.9	Val 78, Arg 305, Pro 334(2), Thr 336	1.95, 4.05, 1.81, 2.04, 2.18
16.	Deoxycytidine	−6.4	Glu 80, Leu 81, Arg 256, Met 340	1.92, 2.28, 4.72, 2.64
17.	5-hydroxy-7-[4-hydroxy-2-methoxy-3-(3-methylbut-2-enyl)phenyl]-2,2-dimethyl-7,8-dihydropyrano[3,2-g]chromen-6-one	−6.4	Gly 337	2.09
18.	Adenosine	−6.3	Glu 80, Arg 256, Pro 334	2.52, 6.44, 1.98
19.	N-Acetyl Phenylalanine	−6.2	Pro 334, Thr 336, Phe 397	2.04, 2.63, 5.00
20.	Citreorosein	−6.0	Glu 80, Gly 109, His 236	2.09, 2.29, 2.30
21.	2-hydroxy-4-methoxy-3-(3-methylbut-2-enyl)-6-(2-phenylethyl)benzoic acid	−6.0	Thr 336, Gly 337, Phe 397	2.08, 2.70, 4.84
22.	Cortisol	−5.7	Val 78, Glu 223	2.14, 1.83
23.	Caffeate	−5.5	Pro 244, Thr 336, Phe 397	2.75, 2.18, 4.86
24.	N-methylaurotetanine	−5.1	Pro 334	1.62
25.	Phenylalanine	−5.0	Pro 334, Phe 397	2.19, 4.92
26.	Pulvinic acid	−5.0	Arg 256, Thr 336, Gly 337	2.01, 2.28, 2.31
27.	5-Chlorodivaricatinic acid	−4.9	Val 78, Glu 80, Arg 256	2.07, 2.12, 3.53
28.	Glucosaminate	−4.8	Tyr 200, Asp 327, Gly 339, Met 340	2.01, 1.75, 2.49, 2.13
29.	7-methoxy-9,10-dihydrophenanthrene-2,5-diol	−4.8	Pro 334	2.05
30.	p-Coumaric acid	−4.2	Pro 244, Thr 336, Phe 397	2.67, 2.33, 4.89
31.	Paraxanthine	−4.0	Glu 80, Arg 256, Pro 334	1.90, 6.34, 2.17
32.	Lycorine	−4.0	Glu 80, Gly 109, Gly 235, Tyr 248	4.58, 2.32, 1.98, 2.25
33.	Theobromine	−3.9	Glu 80, Leu 81, Met 340	2.21, 2.38, 2.21
34.	(4S,4aR,7aS,9aR)-4,6,6-trimethyl-3-oxo-1,3,4,5,6,7,7a,9a-octahydropentaleno[1,6a-c]pyran-9-carboxylic acid	−3.4	Val 112	2.09
35.	Norepanorin	−3.4	Glu 80, Val 112, Thr 336	2.46, 2.16, 2.06
36.	Allocryptopine	−3.0	Thr 336	1.82
37.	Hexadecanoic acid	−2.9	Gly 339, Met 340	2.04, 2.06
38.	Minoxidil	−2.3	Tyr 248	5.33
39.	Tetradecanoic acid	−2.1	Gly 339, Met 340	2.70, 1.84
40.	11-eicosenoic acid	−2.0	Asp 111, Val 112	2.59, 1.78

(**a**)

(**b**)

(**c**)
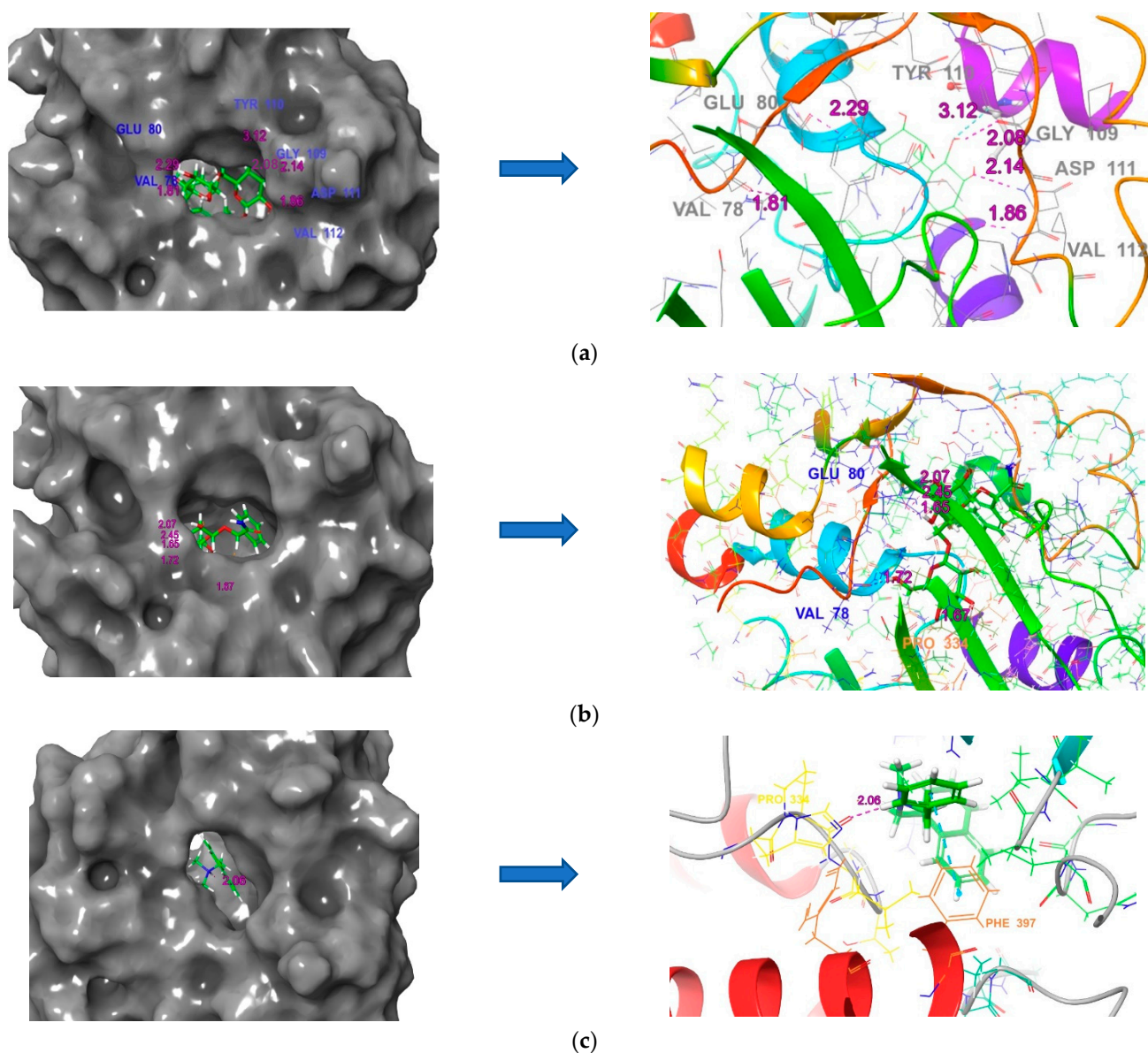
Figure 6. Docked structure of compound (**a**) 56776227, (**b**) 11248520, (**c**) naftifine with squalene epoxidase (SE).

3.7. MMGB-SA Analysis

From the binding free energy calculation studies, the compounds 56776227 and 9826264 have good binding energy values of −51.92 kcal/mol and −47.03 kcal/mol, respectively, which are better than the drug naftifine. The drug molecule has a dG bind value of −40.59 kcal/mol (Table 3).

Table 3. MM-GBSA calculation for selected docked complexes.

S.No	Compound	MMGBSA dG Bind
1.	567776227	−51.92
2.	11248520	−38.08
3.	9826264	−47.03
4.	Naftifine	−40.59

3.8. Molecular Dynamics Simulation

MD simulation is an essential study to realize the steadiness of the ligand's binding attraction while the protein is simulated. The Desmond module of Schrödinger was used to observe the stability of complicated structures of SE with compound 56776227 and SE with the drug naftifine.

3.9. Squalene Epoxidase (SE) with Compound 56776227

The RMSD plot revealed that the docked structure of protein squalene epoxidase and compound 56776227 exposed that the equilibrium of both protein C-alpha atoms and heavy atoms of ligand fluctuated up to the 35th ns. Then, both the atoms did not fluctuate more, and if the time period of the simulation was extended, the equilibrium may be within the adequate range of 3Å. In addition, there were no deviations between the protein and ligand up to the completion of the simulation period (Figure 7a), indicating that this docked structure was steady.
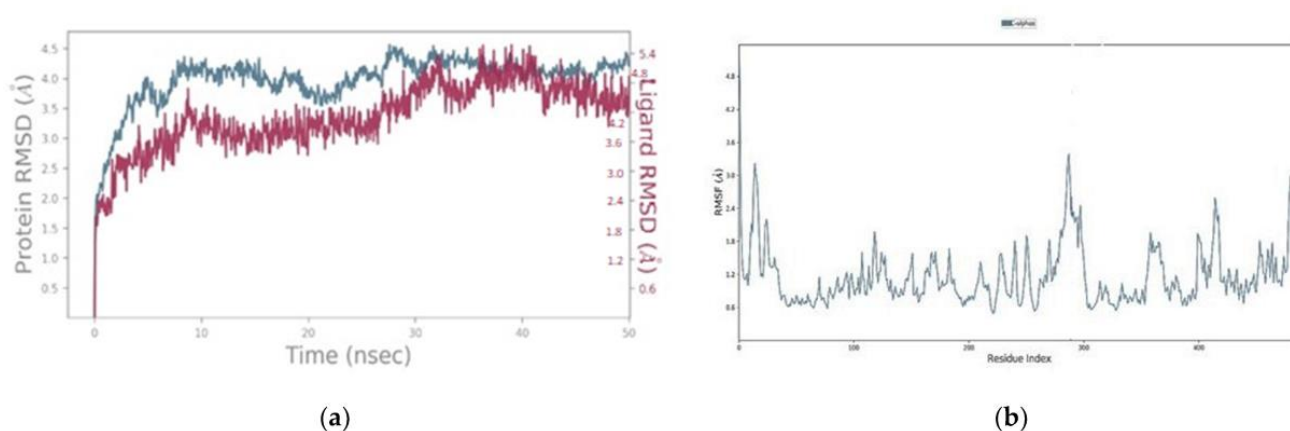
Figure 7. Protein–ligand RMSD (blue color indicates protein C-alpha of SE and red color indicates heavy atoms of 56776227 (**a**) and protein RMSF (**b**) plots of MD simulation results of docked structure of SE with compound 56776227.

The RMSF plot depicts the variation in specific squalene epoxidase protein residues. According to the analysis, the residues around the 10th, 290th, 410th, and 480th were more fluctuated than other residues, but the binding pocket residues were within the permissible range of 3Å (Figure 7b). As a result, the protein was sturdy.

According to the study of the protein–ligand contacts timeline image, the substance 56776227 had preserved the interactions with the residues Glu 80, Gly 109, Gly 235, Leu 246, Tyr 248, Pro 334, and Thr 336 of squalene epoxidase with maximum simulation period (Figure 8a).

The molecule 56776227 interacted via hydrogen bonds with the functionally conserved residues Glu 80, Tyr 110, Pro 334, and Thr 336 and the binding site residues Gly 109 and Cys 136, and had hydrophobic interactions and water bridges with the binding site residues Val 105, Leu 246, and Tyr 248 and Thr 107, Gly 235 and His 236, respectively, as seen in the histogram of protein–ligand contacts (Figure 8b). The 2D image at the 50th ns reveals that the residues Glu 80, Gly 109, Pro 334, and Thr 336 had hydrogen bond interactions, and these interactions maintained the maximum period of the simulation time (Figure 9).

3.10. Naftifine with Squalene Epoxidase

The MD simulation result of the docked complex structure of naftifine with squalene epoxidase reveals that the complex structure was good because the heavy atoms of naftifine were presented within the 2.5 Å and C-alpha atoms of squalene epoxidase steadily after the 27th ns to the end of the simulation period (Figure 10a). From the analysis of RMSF, the residues of squalene epoxidase were within an acceptable area, but some residues fluctuated

more, especially the residues around the 280th, 370th, and 420th positions. However, the residues involved in binding site regions were within the boundary (Figure 10b).
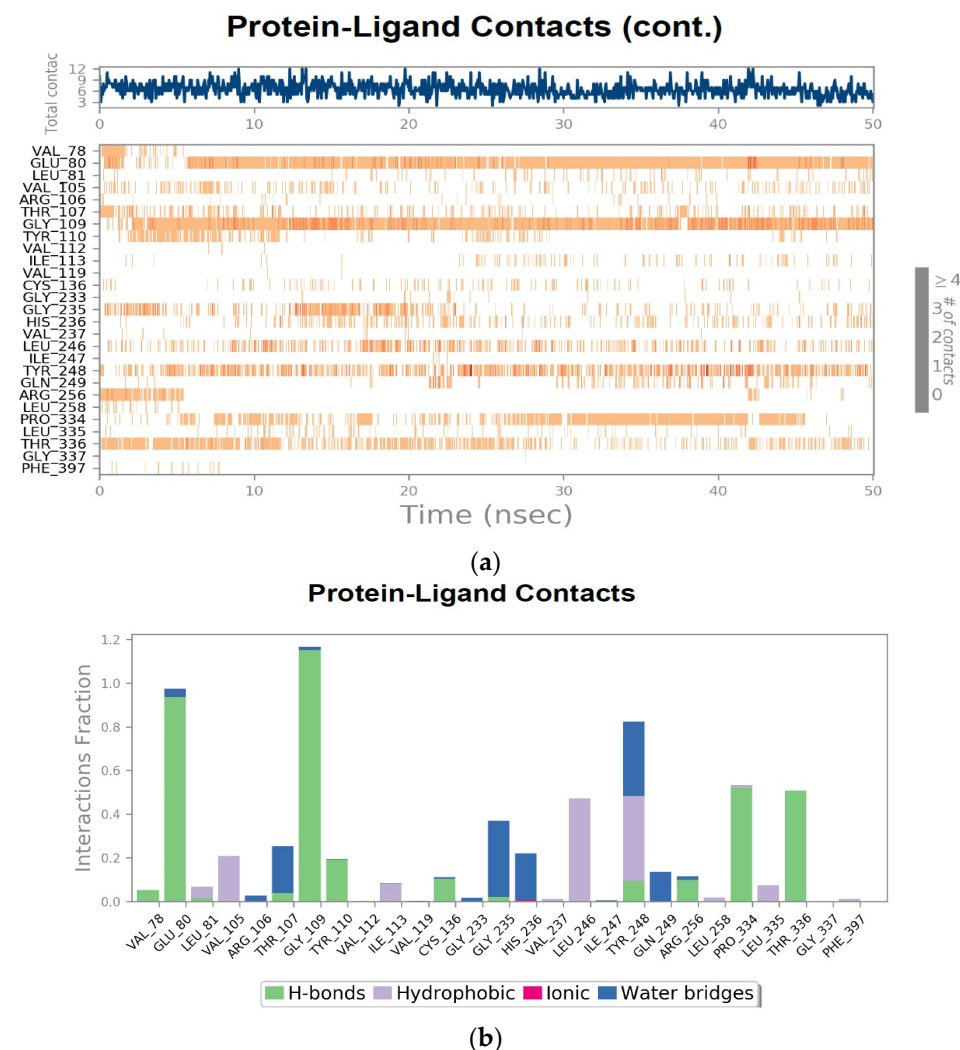

(**a**)

(**b**)

Figure 8. (**a**) Timeline showing ligand interactions with various SE amino acid residues. (**b**) Different contacts between SE and 56776227 over the progress of the MD simulation.
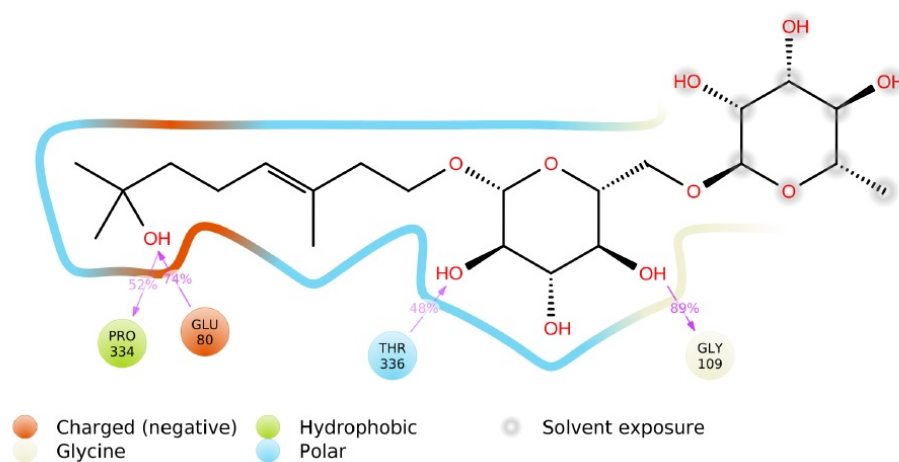

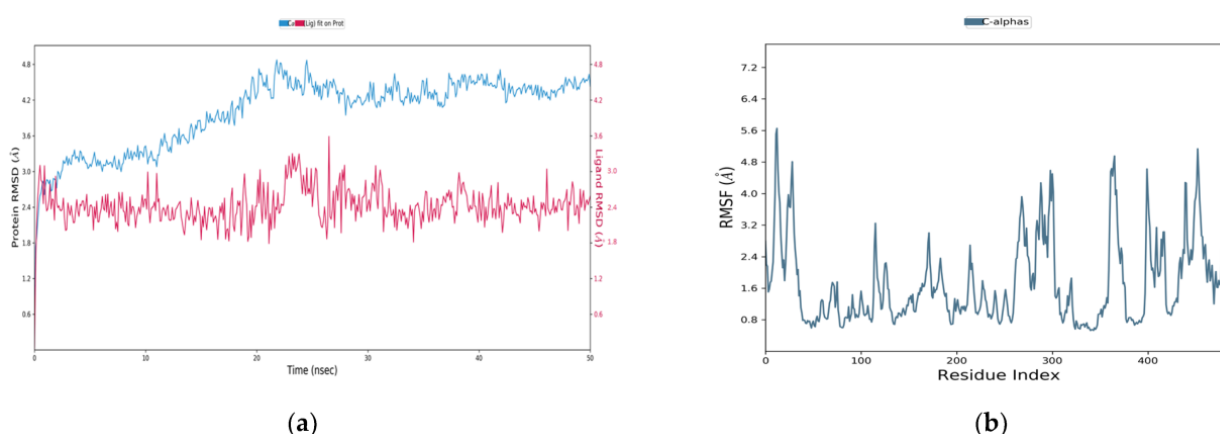**Figure 9.** Interactions of compound 56776227 with SE 50th ns.

(a)   (b)

Figure 10. Protein–ligand RMSD (**a**) and protein RMSF (**b**) plot of MD simulation result of docked structure of SE with compound 56776227.

3.11. Protein–Ligand Interactions

From the timeline plot, the drug molecule naftifine interacted with the functionally conserved residue Glu 80, binding site residues Leu 81, Leu 246, Tyr 248, Leu 258, and Leu 335 of squalene epoxidase (Figure 11a). The histogram plot of protein–ligand contacts showed that the residue Glu 80 had a strong hydrogen bond interaction; Glu 80 had ionic interactions; Leu 81, Tyr 110, Leu 246, Leu 258, His 333, and Leu 335 had hydrophobic interactions; and Pro 334 with water bridges (Figure 11b). The 2D diagram showed that the drug naftifine interacts with Glu 80 and Tyr 248 at the 50th ns, but other than these residues, Leu 81, Leu 246, Leu 258, and Leu 335 had maintained the interactions with naftifine at the maximum time period (Figure 12).
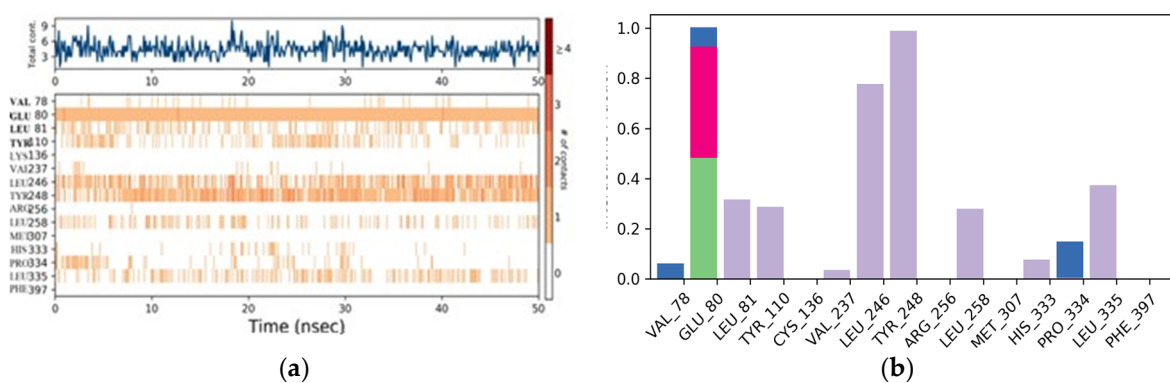

(a)   (b)

Figure 11. (**a**) Timeline showing ligand interactions with various amino acid residues of squalene epoxidase. (**b**) Different contacts between SE and naftifine over the progress of the MD simulation.
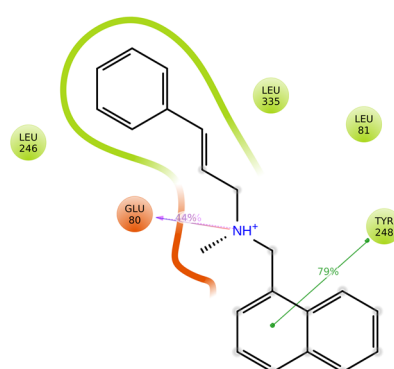

Figure 12. Interactions of drug naftifine with SE at 50th ns.

The docked structure of squalene epoxidase and compound 56776227 was more stable than the docked structure of SE with naftifine, according to the analysis of different MD simulation parameters. According to this research, the substance compound 56776227 effectively inhibits the squalene epoxidase protein in *M. gypseum*.

4. Discussion

Dermatophytes are widely spread all over the world, especially in warm and humid weather countries [28]. Patients all around the world experience socio-physiological issues because of the dangerous superficial infection known as dermatophytoses, so it is important to offer a safer, less expensive course of therapy.

Previous research showed that water and MET extracts of *Balanites aegyptiaca*'s fruit may have probable effects against species of *Aspergillus* and *Candida* [29]. In addition to that, the fruit mesocarp of *B. aegyptiaca*'s fractioned methanol extract had antidermatophytic activity against *M. gypseum* [30].

Additionally, effective antifungal action was present in flavonoids, steroids, and phenolic compounds [31,32]. The fractioned CHL extract of fruit epicarp used in the current research revealed saponins, steroids, flavonoids, and phenols to have antidermatophytic effects against *M. gypseum*.

The squalene epoxidase enzyme turns squalene into squalene oxide. Additionally, the formation of lanosterol and cell membranes depends on this enzyme. Squalene epoxidase was inhibited, which increased squalene accumulation in cell membranes, increased membrane permeability, disruption of cellular processes, and eventually fungal death. The effect of allylamines on ergosterol biosynthesis is similar to that of azoles, but they work at an earlier stage by inhibiting squalene epoxidase [33]. According to Nowosielski et al. (2011) [34] and Yamada et al. (2017) [35], the residues Tyr 90, Val 92, Phe 402, Cys 416, and Phe 420 of squalene epoxidase in *S. cerevisiae* interacted with terbinafine. In molecular docking and molecular dynamics simulation studies, comparable residues from *M. gypseum*, such as Tyr 110, Val 112, and Phe 397, were obtained.

The compounds 56776227, 11248520, and platyphylloside are the top-ranked compounds in docking studies. The chemical substance 56776227 belongs to the fatty acyl glycosides class. The fatty acyl glycosides have potent antimicrobial activity against bacterial and fungal pathogens [36]. Compound 11248520 is another important compound; it is the class of O-acyl carbohydrate. The carbohydrates have significant antifungal and antibacterial activity; especially, they were good inhibitory activity against the protein Lanosterol 14alpha-demethylase [37]. Platyphylloside is a class of diarylheptanoids; it exhibits effective antifungal activity against *Fusarium equiseti*, *F. tricinctum*, *Candida albicans*, and *Saccharomyces cerevisiae* [38] and effective antifungal inhibitor against *T. rubrum* [27].

Compound 56776227 was established to interact with significant squalene epoxidase residues, and RMSD and RMSF values were within the allowable range; this shows that the complex is steady. In addition, Compound 56776227 had maintained the interactions with Glu 80, Gly 109, Tyr 110, Tyr 248, Pro 334, and Thr 336, which were structurally and functionally important residues of squalene epoxidase protein for inhibiting the function of ergosterol biosynthesis pathway in *M. gypseum* [39]. Therefore, this study firmly suggests the antidermatophytic activity of compound 56776227 was superior to that of terbinafine and naftifine; consequently, the effectiveness of this substance against *M. gypseum* will be further investigated.

5. Conclusions

This research study proved that the plant *B. aegyptiaca* has effective medicinal assets by testing an epicarp fractionated chloroform extract against the pathogen *M. gypseum* that causes dermatophytoses. Additionally, in silico research verified that the substances 56776227, 11248520, and 9826264 were extracted from the epicarp, and they interacted with key residues in the *M. gypseum* squalene epoxidase. This research demonstrated the high potential of the compound 56776227 to combat dermatophytes. Further research on

compound 56776227 will be conducted to ascertain its effectiveness through in vitro and in vivo tests against *M. gypseum*.

References

1. Moskaluk, A.E.; VandeWoude, S. Current Topics in Dermatophyte Classification and Clinical Diagnosis. *Pathogens* **2022**, *11*, 957. [CrossRef] [PubMed]
2. Shaoo, A.K.; Mahajan, R. Management of tinea corporis, tine cruris and tinea pedis: A comprehensive review. *Indian Dermatol. Online J.* **2016**, *7*, 77–86.
3. Ginter, G. Ecology, epidemiology and clinical symptomatology of infections due to *Microsporum gypseum*. *Mycoses* **2009**, *32*, 531–535. [CrossRef]
4. Souza, L.K.H.; Oliveira, C.M.A.; Ferri, P.H.; Santos, S.C.; Oliveira Júnior, J.G.; Miranda, A.T.B.; Liao, L.M.; Silva, M.R.R. Antifungal properties of Brazilian cerrado plants. *Braz. J. Microbiol.* **2022**, *33*, 247–249. [CrossRef]
5. Lee, W.J.; Park, J.H.; Kim, J.Y.; Jang, Y.H.; Lee, S.; Bang, Y.J.; Jun, J.B. Low but continuous occurrence of *Microsporum gypseum* infection in the study on 198 cases in South Korea from 1979 to 2016. *Ann. Dermatol.* **2018**, *30*, 427–431. [CrossRef] [PubMed]
6. Dolenc-Voljc, M.; Gasparic, J. Human Infections with *Microsporum gypseum* Complex (Nannizzia gypsea) in Slovenia. *Mycopathologia* **2017**, *181*, 1069–1075. [CrossRef]
7. Chugh, A.; Ray, A.; Gupta, J.B. Squalene epoxidase as hypocholesterolmic drug target revisited. *Prog. Lipid Res.* **2003**, *42*, 37–50. [CrossRef] [PubMed]
8. Sahni, K.; Singh, S.; Dogra, S. Newer topical treatments in skin and nail dermatophytes infections. *India Dermatol. Online J.* **2018**, *9*, 149–158.
9. Ghorbani, A.; Naghibi, F.; Mosaddegh, M. Ethnobotany, ethnopharmacology and drug discovery. *Iran. J. Pharm. Sci.* **2006**, *2*, 109–118.
10. Al-Thobaiti, S.A.; Zeid, I.A. Medicinal properties of desert plants (*Balanites aegyptiaca*)—An overview. *Glob. J. Pharmacol.* **2018**, *12*, 1–12.
11. Grover, R.K.; Moore, J.D. Toxicometric Studies of Fungicides against Brown Rot Organisms *Sclerotinia fructicola* and *S. laxa*. *Phytopathology* **1962**, *52*, 876–880.
12. Maurya, V.K.; Kachhwaha, D.; Bora, A.; Khatri, P.K.; Rathore, L. Determination of antifungal minimum inhibitory concentration and its clinical correlation among treatment failure cases of dermatophytosis. *J. Family Med. Prim. Care* **2019**, *8*, 2577–2581. [PubMed]
13. Rao, U.S.M.; Abdurrazak, M.; Mohd, K.S. Phytochemical screening, total flavonoid and phenolic content assays of various solvent extracts of tepal of *Musa paradisiaca*. *Malays. J. Anal. Sci.* **2016**, *20*, 1181–1190. [CrossRef]
14. Oh, M.; Park, S.; Kim, H.; Choi, G.J.; Kim, S.H. Application of UPLC-QTOF-MS Based Untargeted Metabolomics in Identification of Metabolites Induced inPathogen-Infected Rice. *Plants* **2021**, *10*, 213. [CrossRef]
15. Demarque, D.P.; Dusi, R.G.; Sousa, F.D.M.; Grossi, S.M.; Silverio, M.R.S.; Lopes, N.P.; Espindola, L.S. Mass spectrometry-based metabolomics approach in the isolation of bioactive natural products. *Sci. Rep.* **2020**, *10*, 1051. [CrossRef] [PubMed]

16. Sheik, S.; Sundararajan, P.; Hussain, A.S.Z.; Sekar, K. Ramachandran plot on the web. *Bioinformatics* **2002**, *18*, 1548–1549. [CrossRef] [PubMed]
17. Halgren, T. New method for fast and accurate binding-site identification and analysis. *Chem. Biol. Drug Des.* **2007**, *69*, 146–148. [CrossRef]
18. Ashkenazy, H.; Abadi, S.; Martz, E.; Chay, O.; Mayrose, I.; Pupko, T.; Ben-Tal, N. ConSurf 2016: An improved methodology to estimate and visualize evolutionary conservation in macromolecules. *Nucleic Acids Res.* **2016**, *44*, W344–W350. [CrossRef]
19. Zhang, Q.; Khetan, A.; Er, S. A quantitative evaluation of computational methods to accelerate the study of alloxazine-derived electroactive compounds for energy storage. *Sci. Rep.* **2021**, *11*, 4089. [CrossRef]
20. Hage-Melim, L.I.S.; Federico, L.B.; Oliveria, N.K.S.; Francisco, V.C.C.; Correia, L.C.; Lima, H.B.; Gomes, S.Q.; Barcelos, M.P.; Francischini, I.A.G.; de Paula da Silva, C.H.T. Virtual screening, ADME/Tox predictions and the drug repurposing concept for future use of old drugs against the COVID-19. *Life Sci.* **2020**, *256*, 117963. [CrossRef]
21. Bathula, R.; Muddagoni, N.; Lanka, G.; Dasari, M.; Potlapally, R. Glide Docking, Autodock, Binding Free Energy and Drug-Likeness Studies for Prediction of Potential Inhibitors of Cyclin-Dependent Kinase 14 Protein in Wnt Signaling Pathway. *Biointerface Res. Appl. Chem.* **2022**, *12*, 2473–2488.
22. Ramirez, D.; Caballero, J. Is It Reliable to Use Common Molecular Docking Methods for Comparing the Binding Affinities of Enantiomer Pairs for Their Protein Target? *Int. J. Mol. Sci.* **2016**, *17*, 1–15. [CrossRef] [PubMed]
23. Arokia, A.M.V.; Anantha, K.D.; Hemalatha, M.; Krishnasamy, G.; Ernest, D. In silico studies towards enhancing the anticancer activity of phytochemical Phloretin against cancer drug targets. *Curr. Drug Ther.* **2018**, *13*, 174–188.
24. Liang, D.; Chen, Q.; Guo, Y.; Zhang, T.; Guo, W. Insight into resistance mechanisms of AZD4547 and E3810 to FGFR1 gatekeeper mutation via theoretical study. *Drug Des. Dev. Ther.* **2017**, *11*, 451–461. [CrossRef] [PubMed]
25. Alturki, N.A.; Mashraqi, M.M.; Alzamami, A.; Alghamdi, Y.S.; Alharthi, A.A.; Asiri, S.A.; Ahmad, S.; Alshamrani, S. In-Silico Screening and Molecular Dynamics Simulation of Drug Bank Experimental Compounds against SARS-CoV-2. *Molecules* **2022**, *27*, 4391. [CrossRef]
26. Aier, I.; Varadwaj, P.K.; Raj, U. Structural insights into conformational stability of both wild-type and mutant EZH2 receptor. *Sci. Rep.* **2016**, *6*, 34984. [CrossRef]
27. Abuthakir, M.H.S.; Al-Dosary, M.A.; Hatamleh, A.A.; Alodaini, H.A.; Perumal, P.; Jeyam, M. Platyphylloside, a potential inhibitor from epicarp of B. aegyptiaca against CYP450 protein in T. rubrum—In Vitro and in silico approaches. *Saudi J. Biol. Sci.* **2022**, *29*, 3899–3910. [CrossRef]
28. Al-Janabi, A.A.H.S. Dermatophytosis: Causes, clinical features, signs and treatment. *J. Symptoms Signs* **2014**, *3*, 200–203.
29. Khatoon, R.; Jahan, N.; Ahamed, S.; Shahzad, A. In vitro evaluation of antifungal activity of aerial parts of medicinal plants Balanites aegyptiaca Del. and *Spilanthes acmella* Murr. *J. Appl. Pharm. Sci.* **2014**, *4*, 123–127.
30. Hussain, S.A.M.; Velusamy, S.; Muthusamy, J. Balanites aegyptiaca (L.) Del. for dermatophytoses: Ascertaining the efficacy and mode of action through experimental and computational approaches. *Inform. Med. Unlocked* **2019**, *15*, 100177. [CrossRef]
31. Ayala-Zavala, J.F.; Silva-Espinoza, B.A.; Cruz-Valenzuela, M.R.; Villegas-Ochoa, M.A.; Esqueda, M.; González-Aguilar, G.A.; Calderón-López, Y. Antioxidant and antifungal potential of methanol extracts of Phellinus spp. from Sonora, Mexico. *Rev. Iberoam. De Micol.* **2012**, *29*, 132–138. [CrossRef]
32. Dos Santos, E.C.F.; da Silva, W.A.V.; Machado, J.C.B.; Ferreira, M.R.A.; Soares, L.A.L. Evaluation of the Antioxidant and Antifungal Actions of the Optimized Crude Extract and Fractions from the Aerial Parts of *Acanthospermum hispidum*. *Biopharm. Drug Dispos.* **2022**, *20*, e202200905.
33. Halat, D.H.; Younes, S.; Mourad, N.; Rahal, M. Allylamines, Benzylamines, and Fungal cell permeability: A review of mechanistic effects and usefulness against fungal pathogens. *Membranes* **2022**, *12*, 1171. [CrossRef] [PubMed]
34. Nowosielski, M.; Hoffmann, M.; Wyrwicz, L.S.; Stepniak, P.; Plewczynski, D.M.; Lazniewski, M.; Ginalski, K.; Rychlewski, L. Detailed mechanism of squalene epoxidase inhibition by terbinafine. *J. Chem. Infect. Model* **2011**, *51*, 455–462. [CrossRef] [PubMed]
35. Yamada, T.; Maeda, M.; Alshahni, M.M.; Tanaka, R.; Yaguchi, T.; Bontems, O.; Salamin, K.; Fratti, M.; Monod, M. Terbinafine Resistance of *Trichophyton* Clinical Isolates Caused by Specific Point Mutations in the Squalene Epoxidase Gene. *Antimicrob. Agents Chemother.* **2017**, *61*, e00115-17. [CrossRef]
36. Bournonville, C.G.; Filippone, M.P.; Peto, P.d.L.D.; Trejo, M.F.; Couto, A.S.; de Marchese, A.M.; Ricci, J.C.D.; Welin, B.; Castagnaro, A.P. Strawberry fatty acyl glycosides enhance disease protection, have antibiotic activity and stimulate plant growth. *Sci. Rep.* **2020**, *10*, 8196. [CrossRef] [PubMed]
37. Kawsar, S.M.A.; Almalki, F.A.; Ben Hadd, T.; Laaroussi, H.; Khan, M.A.R.; Hosen, M.A.; Mahmud, S.; Aounti, A.; Maideen, N.M.P.; Heidarizadeh, F.; et al. Potential antifungal activity of novel carbohydrate derivatives validated by POM, molecular docking and molecular dynamic simulations analyses. *Mol. Simul.* **2022**, *48*, 60–75. [CrossRef]
38. Novakovic, M.M.; Novakovic, I.; Cvetkovic, M.; Tesevic, V. Antimicrobial activity of the diarylheptanoids from the black and green alder. *Braz. J. Bot.* **2015**, *38*, 441–446. [CrossRef]
39. Jorda, T.; Puig, S. Regulation of Ergosterol Biosynthesis in *Saccharomyces cerevisiae*. *Genes* **2020**, *11*, 795. [CrossRef]